

Multiple Conformations of the Metal-Bound Pyoverdine PvdI, a Siderophore of *Pseudomonas aeruginosa*: A Nuclear Magnetic Resonance Study^{†,‡}

Emeric Wasielewski,[§] Der-Lii Tzou,[△] Baudoin Dillmann,[§] Jerzy Czaplicki,[⊥] Mohamed A. Abdallah,[#]
R. Andrew Atkinson,[§] and Bruno Kieffer^{*§}

Laboratoire de Biologie et de Génomique Structurales, Biomolecular NMR group, IGBMC UMR 7104 CNRS, ESBS, bd Sébastien Brandt BP 10413, 67404 Illkirch Cedex, France, Institute of Chemistry, Academia Sinica, 128 Yen-Chiu-Yuan Road, Sec. 2, Nankang, Taipei 115, Taiwan, Republic of China, Université Paul Sabatier/Institut de Pharmacologie et de Biologie Structurale CNRS, 205, route de Narbonne, 31077 Toulouse, France, and Département Récepteurs et Protéines Membranaires, UMR 7175 École Supérieure de Biotechnologie de Strasbourg, Bd Sébastien Brant, BP 10413 F-67412 Illkirch Cedex, France

Received November 6, 2007; Revised Manuscript Received January 26, 2008

ABSTRACT: Under iron-deficient conditions, the Gram-negative bacterium *Pseudomonas aeruginosa* ATCC 15692 secretes a peptidic siderophore, pyoverdine PvdI, composed of an aromatic chromophore derived from 2,3-diamino-6,7-dihydroxyquinoline and a partially cyclized octapeptide, D-Ser-L-Arg-D-Ser-L-FoOHOrn-(L-Lys-L-FoOHOrn-L-Thr-L-Thr), in which the C-terminal carboxyl group forms a peptidic bond with the primary amine of the L-Lys side chain. In aqueous solution at room temperature, the ¹H NMR spectrum of pyoverdine PvdI-Ga(III) showed clear evidence of exchange broadening. At 253 K, two distinct conformations were observed and the measurement of structural constraints was possible. The three-dimensional structures of the two PvdI-Ga(III) conformers were determined, and analysis of the structures indicates that the observed conformational exchange involves a stereoisomerization of the metal binding coordination accompanied by a change in the global shape of the siderophore. This conformational transition was further characterized by heteronuclear relaxation experiments. The possible implications of this dynamic behavior for siderophore recognition by the receptor FpvAI are discussed.

Iron is an essential element for the growth of many microorganisms (for a review, see ref 1), catalyzing electron transfer in a number of key reactions. Under iron-deficient conditions, many Gram-negative bacteria synthesize and secrete low-molecular weight compounds, termed “siderophores”, into their environment (2). These molecules possess a high affinity for ferric ions that allows them to solubilize iron and deliver it to the bacterial cell. Siderophore–ferric ion complexes bind to a specific outer membrane receptor prior to translocation of the metal ion into the periplasm using an ATP-dependent transport system (3). Despite the recent determination of several three-dimensional structures of such receptors, the structural determinants of the siderophores that are recognized by the receptors as well as the mechanism of translocation remain elusive. The widespread bacteria *Pseudomonas* produce yellow-green siderophores, known as pyoverdines (Pvd). More than 100 different Pvd have been

identified so far, representing a wide class of siderophores. Pvd are chromopeptides composed of a chromophore derived from 2,3-diamino-6,7-dihydroxyquinoline and a peptide moiety that may be linear, partially cyclized, or fully cyclized (4, 5). The chromophore chelates Fe³⁺ ions via its catechol group and via two further bidentate chelating groups harbored by the peptidic chain, typically by hydroxyaspartic acid and/or hydroxyornithine residues. The site at which the peptidic chain is attached to the nonaromatic ring of the chromophore and the composition and sequence of the peptidic chain differ among bacteria, suggesting that these differences are responsible for attaining specificity for their outer membrane receptor, while maintaining an exceptionally high affinity for Fe³⁺ ions. The variety in the primary sequence of the peptidic moieties results in a large polymorphism of these siderophores, which is apparent from the small number of three-dimensional structures currently available. This polymorphism derives both from the conformation of the peptidic chain and from the absolute configuration of the octahedral coordination of the metal ion. Both ferric pseudobactin from *Pseudomonas* B10 (6) and pyoverdine GM-II from *Pseudomonas fluorescens* (7) have Δ configurations, while pyoverdine G4R from *Pseudomonas putida* (8) and azoverdin (9), an iso-pyoverdine from *Azomonas macrocytogenes*, have Δ configurations.

Pseudomonas aeruginosa ATCC 15692 produces a pyoverdine (Figure 1), PvdI,¹ which is considered to be an

[†] This work was supported by the CNRS together with the Taiwan NSC (NSC-95-2113-M-001-015) and the French ministry of foreign affairs, whose support allowed fruitful scientific exchanges. E.W. was supported by a grant from Ministère de l'Enseignement Supérieur, de la Recherche et de la Technologie.

[‡] Structures have been deposited in the BMRB database as entries 15629 and 15630 for A conformers and entry 15631 for the B conformer.

* To whom correspondence should be addressed. E-mail: kieffer@esbs.u-strasbg.fr. Telephone: 33390244722. Fax: 33390244718.

[§] IGBMC UMR 7104 CNRS.

[△] Academia Sinica.

[⊥] Université Paul Sabatier/Institut de Pharmacologie et de Biologie Structurale CNRS.

[#] UMR 7175 École Supérieure de Biotechnologie de Strasbourg.

¹ Abbreviations: PvdI, pyoverdine produced by *P. aeruginosa* (also named PaA in previous publications); rms, root-mean-square.

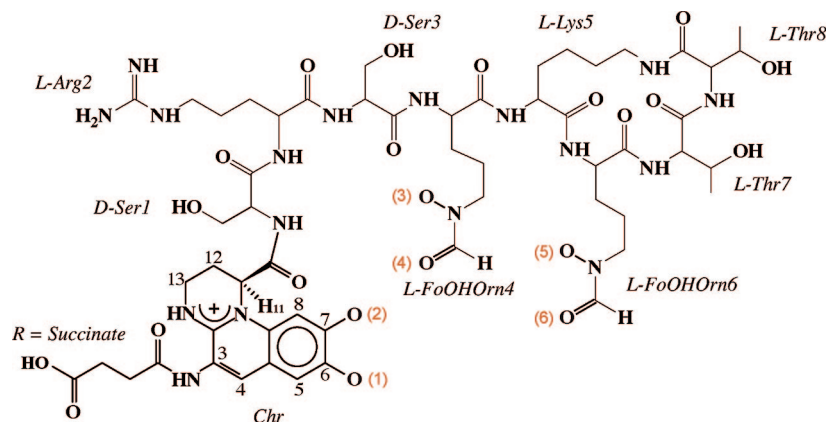


FIGURE 1: Chemical structure of pyoverdine PvdI from *P. aeruginosa*. Standard three-letter codes are used for amino acids, except for *N*-formyl-*N*-hydroxyornithine (FoOHOrn). Metal coordination sites are numbered from (1) to (6). Two forms of PvdI are secreted which differ in the nature of the R group linked to the C3 atom of the chromophore. The major form of PvdI contains a succinate group and was formerly known as PaA.

essential factor for virulence and which is composed of a partially cyclized octapeptide attached to the 2,3-diamino-6,7-dihydroxyquinoline-based chromophore (10). The chromophore is identical to that of other pyoverdines, such as pyoverdine G4R from *P. putida*, while the octapeptide has the composition D-Ser-L-Arg-D-Ser-L-FoOHOrn-(L-Lys-L-FoOHOrn-L-Thr-L-Thr), in which the carboxyl group of the C-terminal L-Thr8 residue forms a peptidic bond with the primary amine of the L-Lys5 side chain. Two different groups may be found attached to the chromophore at the C3 position, the major one being a succinate group (form A also known as PaA).

Detailed studies of the interaction of PvdI and PvdI analogues with the receptor FpvAI using FRET have shown that the receptor binds both apo PvdI as well as metal ion-complexed PvdI (11–13), and the three-dimensional structures of the outer membrane receptors complexed with both these forms of PvdI have been reported (14, 15). These structural studies revealed the possible importance of the molecular flexibility of the peptide chain of PvdI in the recognition mechanism (16). In an attempt to understand the structural and dynamical properties of PvdI that may be important for molecular recognition, we have undertaken a detailed structural study of PvdI-Ga(III), in which the Ga³⁺ ion is used as a diamagnetic isosteric substitute for Fe³⁺. Early NMR studies of pyoverdine PvdI-Al(III) suggested the presence of two conformers in solution (17), and two conformers of PvdI-Cr(III) could be separated chromatographically (18). In addition, fluorescence studies have shown that FpvAI binds PvdI-Ga(III) and PvdI-Fe(III) with the same affinity (7–16 nM) (19). We were able to obtain complete ¹H, ¹³C, and ¹⁵N resonance assignments for the two conformers of PvdI-Ga(III) with the combined use of triple-resonance experiments and cryosolvents (20). Here, we report the three-dimensional structures of the two PvdI-Ga(III) conformers and suggest that the observed conformational exchange involves stereoisomerization of the metal binding coordination. The possible implications of this dynamic behavior for siderophore recognition by the receptor are discussed.

EXPERIMENTAL PROCEDURES

NMR Spectroscopy. Experimental details of sample preparation and spectra acquisition have been reported previously

(20). NMR experiments were carried out on a Bruker DRX 600 MHz NMR spectrometer between 293 and 253 K. Internuclear distances were obtained from the analysis of NOE buildup curves measured using an unlabeled sample of PvdI-Ga(III). A set of 17 homonuclear two-dimensional (2D) NOESY spectra were recorded at 264 K with mixing times ranging from 20 to 500 ms, and a further set of eight homonuclear 2D NOESY spectra was recorded at 253 K with mixing times ranging from 10 to 250 ms. ³J_{HN-Hα} coupling constants were measured at both temperatures from a set of two-dimensional ¹H–¹⁵N CT-HMQC-J spectra (21). Relaxation measurements were performed at 253 K using the pulse sequences proposed by Farrow et al. (22). A set of nine experiments was recorded to describe the decay of longitudinal and transverse ¹⁵N magnetization with relaxation delays of 5, 42, 83, 165, 256, 328, 655, 1310, and 1550 ms for the longitudinal relaxation rate (*R*₁) and 20, 40, 60, 75, 80, 100, 120, 140, and 150 ms for the transverse relaxation rate (*R*₂). Experiments with relaxation delays of 256 ms (for *R*₁) and 75 ms (for *R*₂) were recorded twice. ¹H–¹⁵N heteronuclear NOEs were determined using two experiments, with and without proton saturation. The intensities of the ¹H–¹⁵N correlation peaks were measured using FELIX 2.1 (Biosym Technologies, San Diego, CA). Both relaxation rates and ³J_{HN-Hα} values were extracted from nonlinear fits of the time-dependent intensities using MATLAB (The MathWorks Inc., Natick, MA). Statistical errors were estimated using Monte Carlo simulations.

Interproton Distance Measurements. In the presence of conformational exchange, the extraction of distances from NOE buildup curves must be performed with particular caution, since the time-dependent evolution of the measured intensity is multiexponential. Systematic errors in the measured distances resulting from neglect of the exchange contribution to the NOE cross-peak were quantified using MATLAB scripts. At 253 K, the conformational exchange rate is in the range of 1–2 s^{−1} and the large correlation time of the molecule (9 ns) leads to large interproton cross-relaxation rates. For two protons that are 2.5 Å apart, the cross-relaxation rate is −2.0 s^{−1}. Under these conditions, direct conversion of the initial slopes of NOE buildup curves (mixing times of <70 ms) into distances leads to an overestimation of the distances by 10%, which was consid-

ered to be acceptable. The error increases to 25% for larger distances (3.5–4.5 Å). The set of measured distances was further validated by examining the distribution of sequential distances along the backbone and their consistency with the theoretical range and, for intraresidue H_N-H_α distances, with measured $^3J_{HN-H\alpha}$ coupling constants. An upper tolerance of 0.40 Å was assigned to all distances, increased by a further 0.40 Å for each pseudoatom involved in the distance. An increase in the upper distance bound by 0.40 Å was used for pairs of protons displaying nonlinear buildup curves. The longest distances were limited to 5.0 Å with an upper tolerance of 0.80 Å. For all distances, the lower bound was fixed to 1.80 Å.

Structure Calculations. Structure calculations used standard protocols (sa, refine, accept) in XPLOR-NIH (23). Standard topology and parameter files (topallhdg.pro and parallhdg.pro) were modified to allow definition of the chromophore and the two nonstandard L- δ N-formyl- δ N-hydroxyornithines (L-FoOHOrn) residues of PvdI. Nonbonded parameters for the gallium(III) ion were set to the same values used for the iron(III) ion in standard XPLOR-NIH parameters sets, since the radii of the two ions are similar.

The first stage of calculations was performed using a simulated annealing protocol performing 12000 steps at a high temperature (2000 K) and a further 12000 steps cooling to 100 K, with a time step of 1 fs for integration of the equations of motion. At this stage, the only structural restraints applied were those that define the octahedral geometry of the metal coordination site, to generate a set of all 16 possible stereoisomers of PvdI-Ga(III). The coordination of the Ga(III) ion was defined using distance restraints between the metal ion and each of the six coordinating oxygen atoms (Chr O6, Chr O7, L-FoOHOrn4 O ϵ , L-FoOHOrn4 O ζ , L-FoOHOrn6 O ϵ , and L-FoOHOrn6 O ζ). These distances were set to 2.04 Å (± 0.10 Å), covering the range of values found in crystallographic studies of siderophores. Distances between pairs of coordinating oxygen atoms on adjacent vertices of the octahedron were set to 2.85 Å (± 0.10 Å). A force constant of 50.0 kcal mol $^{-1}$ Å $^{-2}$ was applied to all of these distance restraints. Additional improper angles were used to fix the metal ion in chelating group planes and set to 0° or 180° ($\pm 20^\circ$). Each coordination geometry was imposed using three improper angle restraints between sets of four coordinating oxygen atoms set to $\pm 54.8^\circ$ ($\pm 15^\circ$).

In the second stage of calculations, the resulting structures were refined using all experimental restraints. These structures were subjected to 6000 steps of cooling from 2000 to 100 K, followed by 1400 steps of energy minimization. All distance restraints were applied using a square-well NOE energy function (24). During this stage, the restraints defining the geometry of metal coordination were scaled by a factor of 10 relative to the experimental restraints to ensure that the correct geometry was maintained. The quality of the final structures was assessed by analysis of violated experimental restraints. To further assess the consistency of the PvdI-Ga(III) models with the NOE data set, an agreement factor f_A was calculated for each structure as follows:

$$f_A = \sum_{i=1}^{N_d} \frac{a_i}{d_i^6}$$

where N_d is the number of interproton distances, d_i , of <4 Å in the structure and a_i is equal to 0 if the short distance, d_i , corresponds to an experimental cross-peak or 1 if not. This factor increases with the number of unobserved short distances and allows rejection of structures that are not consistent with experimental data. Structures were visualized with MolMol 2.6 (25). The family of structures was selected when at least one-fourth of the calculated structures were found to fulfill the following acceptance criteria (no violation greater than 0.5 Å, 10°, 0.5 Hz, 0.01 Å, and 2° for the distance, dihedral angle, coupling constant, bond, and bond angle restraints, respectively).

RESULTS

1H NMR spectra of pyoverdine PvdI-Ga(III) recorded at room temperature were characterized by broad resonances indicative of intermediate exchange, while at lower temperatures, two sets of resonances could be distinguished. The combined use of cryosolvents and triple-resonance NMR techniques allowed the assignments of the resonances of 1H , ^{15}N , and ^{13}C nuclei of two exchanging conformers of pyoverdine PvdI-Ga(III) to be obtained at 264 and 253 K (20). The exchange kinetics were investigated further to determine the optimal temperature for extraction of structural information for both conformers.

Conformational Exchange Kinetics for Pyoverdine PvdI-Ga(III). For the amide protons of L-Arg2 and D-Ser3, unaffected by spectral overlap, integration of the volumes of diagonal and pure exchange correlation peaks in NOESY spectra recorded with different mixing times provided data that could be fitted to a two-site exchange model (Figure 2A). Analysis of the exchange rates extracted from sets of spectra recorded between 278 and 253 K (Figure 2B) yielded the enthalpic and entropic terms of the activation energy for conformational exchange. The values ($\Delta H^* = 83 \pm 10$ kJ/mol; $\Delta S^* = 0.3 \pm 0.07$ kJ K $^{-1}$ mol $^{-1}$) suggest that pyoverdine PvdI-Ga(III) undergoes a major structural change during the exchange. At 253 K, the chemical exchange rate is in the range of 1.2–2.0 s $^{-1}$, a rate that slightly exceeds the longitudinal relaxation rates of all protons of the molecule, allowing conformation-specific cross-relaxation rates to be measured and the structural changes between the two conformations to be characterized. The impact of conformational exchange on the accuracy of distances derived from spectra recorded at 253 K was assessed using a modeling procedure in which NOE intensities were calculated using a 4×4 relaxation matrix for two spins involved in two-state exchange, and derived distances compared to the true distances between the spins. The simulations showed that neglect of conformational exchange leads to an increase in the experimental error in the derived distance of ca. 15%, increasing to 25% for two spins separated by a short distance in both conformations (see Table S1 of the Supporting Information). These results were incorporated into the structure calculation procedure.

Experimental Restraints for Exchanging Conformers. NOE buildup curves from NOESY spectra with different mixing times recorded at 253 K were used to generate a set of short

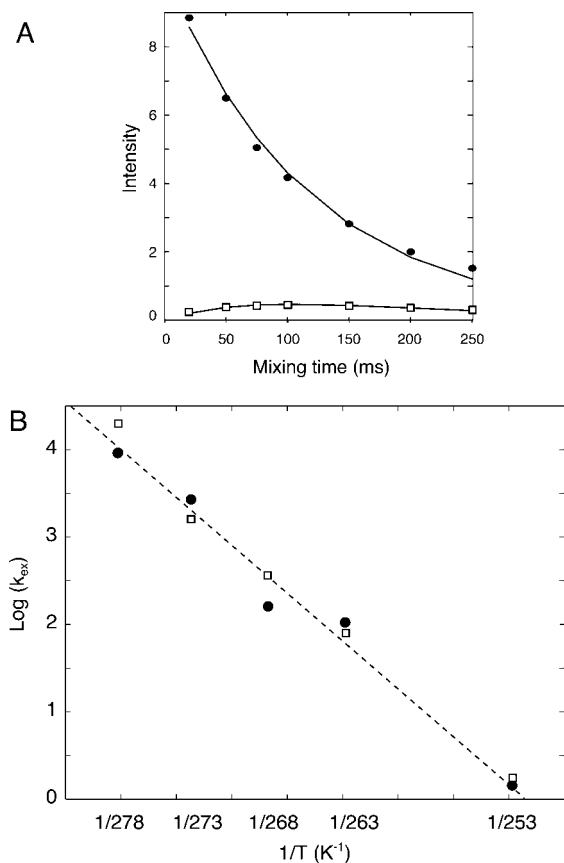


FIGURE 2: (A) Example of nonlinear fitting of the time-dependent evolution of the diagonal peak (●) and B (□), and the cross-peak due to chemical exchange obtained for the amide proton of L-Arg2. B: Temperature-dependent evolution of the measured chemical exchange rate, k_{ex} , obtained for residues L-Arg2 (●) and D-Ser3 (□). The linear fit for L-Arg2 is depicted using a gray dotted line. These data were obtained by fitting the time-dependent NOESY cross-peaks at five different temperatures (278, 273, 268, 264, and 253 K).

intramolecular distances for each conformer of pyoverdine PvdI-Ga(III) (Table 1), assuming a single rotational correlation time for all interproton vectors of the molecule. The rotational correlation time was measured, using the fixed distance between the H4 and H5 protons of the chromophore as a reference, and its value, 9.3 ns, found to be compatible with the size of the molecule, the temperature, and the viscosity of the cryosolvent. Many distances were found to

Table 1: Summary of Experimental Restraints Used for Three-Dimensional Structure Calculations of Conformers A and B of PvdI-Ga(III)

	form A	form B
experimental restraints		
total no. of NOE restraints	92	82
intraresidue	8	8
sequential ($ i - j = 1$)	52	44
medium-range ($1 < i - j \leq 4$)	32	30
HN-HN restraints	9	9
HN-aliphatic restraints	53	49
aliphatic restraints	30	24
no. of hydrogen bond restraints	0	0
no. of dihedral angle restraints	5	3
no. of $^3J_{HN-H\alpha}$ couplings	6	5
no. of additional restraints for the coordination site		
dihedral angle restraints	9	9
O-Ga bond restraints	6	6
O-O bond restraints	9	9

Table 2: Values of $^3J_{HN-H\alpha}$ Coupling Constants (hertz) Measured at 253 K

residue	conformer A	conformer B
Chr	4.3 ± 1.5	4.4 ± 1.3
D-Ser1	3.9 ± 2.1	5.2 ± 2.7
L-Arg2	9.3 ± 0.1	8.7 ± 0.1
D-Ser3	5.9 ± 0.1	4.6 ± 0.1
L-FoOHOrn4	8.9 ± 0.1	6.9 ± 5.3
L-Lys5	8.4 ± 0.1	4.0 ± 2.6
L-FoOHOrn6	6.2 ± 3.7	not determined
L-Thr7	8.4 ± 2.9	7.9 ± 1.6
L-Thr8	7.4 ± 0.1	8.5 ± 3.3

be identical between conformers within experimental error, but a set of 15 distances were found to differ by more than 0.75 Å while further sets of 19 and 15 short distances were found only in conformers A and B, respectively, reflecting two distinct conformations for PvdI-Ga(III). Most of the differences between the sets of distances were localized in the vicinity of L-Arg2 and D-Ser3 and within the macrocycle formed by the peptide bond between the carboxyl group of the C-terminal residue L-Thr8 and the side chain of L-Lys5. Changes in the sets of distances involving the side chain of L-Lys5 indicated a major rearrangement of this macrocycle. For structure calculations, distance restraints were complemented by dihedral angle restraints derived from the measurements of $^3J_{HN-H\alpha}$ coupling constants using constant-time $^1H-^{15}N$ HMQC-J experiments (Table 2). Most of the residues exhibited similar $^3J_{HN-H\alpha}$ values in each conformer, with the notable exception of L-Lys5 with values of 8.4 and 4.0 Hz (Figure 3), indicating a change in dihedral angle φ for this residue. Qualitative analysis of $^3J_{H\alpha-H\beta}$ coupling constants together with intraresidual NOE patterns allowed stereospecific assignments of H β protons for L-FoOHOrn4 and L-Lys5 to be obtained, and the corresponding χ_1 dihedral angles were restrained to the appropriate rotamer value.

Three-Dimensional Structures of PvdI-Ga(III). The strategy adopted for the determination of the three-dimensional structures of PvdI-Ga(III) was similar to that used for the determination of the structure of azoverdin-Ga(III) (9), a siderophore with similar metal ion coordination via two

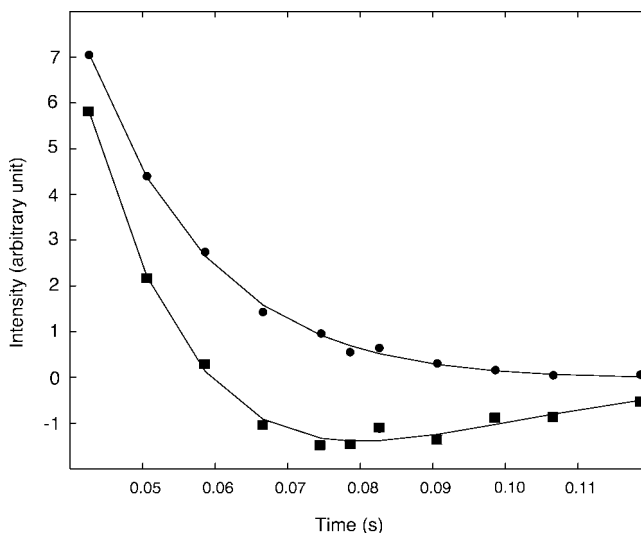
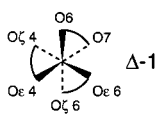
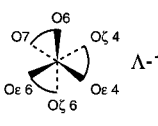
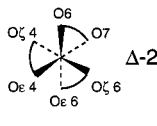
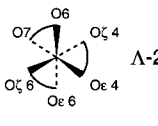
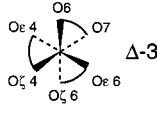
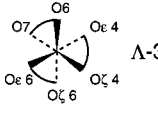
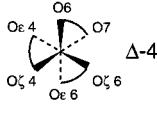
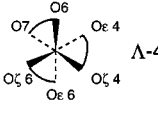
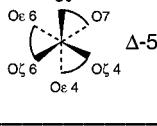
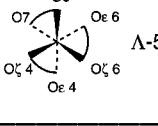
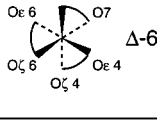
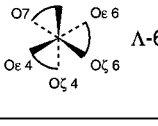
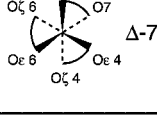
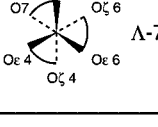
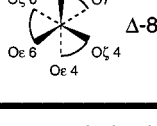
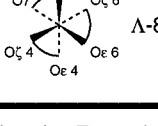


FIGURE 3: Evolution time of $^1H-^{15}N$ peak intensities for L-Lys5 in conformers A (■) and B (●), measured with $^1H-^{15}N$ CT-HMQC-J spectra showing a clear rotation around the N-C α bond of this residue upon conformational exchange. The fits are indicated by solid lines.

Table 3: Results of PvdI-Ga(III) Structure Calculations, for Conformers A and B^a

Δ ISOMERS	A Conformer	B Conformer	Λ ISOMERS	A Conformer	B Conformer
 Δ -1	168.2 3.1 0.206 245 \pm 64 1440 \pm 1025 0	48.5 2.4 0.128 98 \pm 34 746 \pm 642 0	 Λ -1	43.1 5.9 0.081 22 \pm 30 69 \pm 90 4	54.9 5.0 0.106 109 \pm 26 1323 \pm 972 0
 Δ -2	210.2 9.9 0.293 277 \pm 30 1054 \pm 306 0	71.2 2.6 0.082 102 \pm 13 454 \pm 495 0	 Λ -2	42.5 1.6 0.283 119 \pm 47 641 \pm 309 2	39.0 211.8 0.071 56 \pm 13 895 \pm 596 0
 Δ -3	267.7 10.7 0.092 321 \pm 37 1277 \pm 783 0	99.8 2.7 0.176 124 \pm 13 1537 \pm 870 0	 Λ -3	48.7 6.3 0.256 114 \pm 56 1382 \pm 1086 2	45.1 602.3 0.049 60.1 \pm 9.9 1138.0 \pm 1008.0 0
 Δ -4	211.2 7.0 0.408 342 \pm 74 1505 \pm 750 0	97.6 4.9 0.214 116 \pm 10 1355 \pm 1006 3	 Λ -4	62.9 195.3 0.108 127 \pm 51 1122 \pm 850 0	32.1 1.2 0.073 32 \pm 19 95 \pm 55 8
 Δ -5	68.3 109.8 0.346 116 \pm 26 798 \pm 341 0	38.7 116.4 0.035 63 \pm 15 813 \pm 650 2	 Λ -5	94.5 6.8 0.127 142 \pm 42 1070 \pm 978 0	42.7 110.1 0.131 54 \pm 7 1223 \pm 829 2
 Δ -6	142.1 4.5 0.322 173 \pm 19 1201 \pm 683 0	131.3 107.3 0.350 159 \pm 28 1363 \pm 538 0	 Λ -6	138.5 3.0 0.134 246 \pm 58 1604 \pm 1330 0	131.2 203.9 0.118 158 \pm 19 921 \pm 592 0
 Δ -7	27.4 0.8 0.133 21 \pm 20 73 \pm 65 6	130.6 307.7 0.107 150 \pm 13 1455 \pm 624 0	 Λ -7	210.2 6.9 0.372 283 \pm 46 1371 \pm 853 0	139.7 300.5 0.188 181 \pm 29 1180 \pm 552 0
 Δ -8	25.9 0.9 0.139 29 \pm 3 99 \pm 10 14	43.1 124.3 0.178 63 \pm 9 1150 \pm 688 2	 Λ -8	175.3 9.6 0.486 212 \pm 28 1275 \pm 1104 0	44.6 392.1 0.111 65 \pm 10 14756 \pm 785 2

^a Thirty structures were calculated for each isomer of the metal coordination site. For each isomer, the following are reported: NOE energy, $^3J_{\text{HN-H}\alpha}$ coupling constant energy, and agreement factor of the structure with the lowest NOE energy (f_{Λ}). The following numbers are the average global and NOE energies of the 10 best structures and the number of accepted structures of the 30 generated structures. Isomers Δ 8 and Λ 4 have been selected as the best representatives for conformers A and B, respectively (numbers for these isomers are highlighted with a black frame).

hydroxyornithine residues and the catechol moiety of the chromophore. Since the bidentate chelating groups of hydroxyornithine residues lie at the end of a side chain with four rotatable bonds, a systematic search over all absolute configurations of the coordination sphere (16 structures for each conformer) was necessary to fully explore the conformational space. Following the simulated annealing procedure, structures were selected according to their NOE and dihedral angle restraint energies. At this stage, several configurations of each conformer gave satisfactory energy values: isomers

Λ 1, Λ 2, Λ 3, Δ 7, and Δ 8 for conformer A and Λ 4, Λ 5, Δ 4, Δ 5, and Δ 8 for conformer B (Table 3). To further refine the set of PvdI-Ga(III) structures compatible with experimental measurements, short-range distances were calculated for each model and compared to the NOE-derived distances. An agreement factor f_a was used to discriminate against models for which predicted cross-peaks are not observed in NOESY spectra. Analysis of this agreement factor together with the quality of the convergence (reflected by the numbers of accepted structures and the rms deviation of the NOE energy)

Table 4: Structural Statistics^a of Accepted PvdI Structures

	form A		formB
isomer	Δ -7	Δ -8	Λ -4
no. of structures	6	10	8
rms deviation from ideal covalent geometry			
angles (deg)	0.971 ± 0.07	0.889 ± 0.05	0.871 ± 0.119
bonds (Å)	0.0068 ± 0.0007	0.0061 ± 0.0002	0.0065 ± 0.0006
couplings (Hz)	0.094 ± 0.047	0.071 ± 0.011	0.101 ± 0.017
dihedral angles (deg)	0.67 ± 0.24	0.13 ± 0.15	0.27 ± 0.52
improper angles (deg)	1.05 ± 0.2	1.05 ± 0.1	0.90 ± 0.2
NOE restraints (Å)	0.08 ± 0.01	0.07 ± 0.003	0.091 ± 0.01
final energies (kcal/mol)			
E_{overall}	72 ± 65	98 ± 9	95 ± 55
E_{angles}	27 ± 24	38 ± 4	30 ± 18
E_{bonds}	5.0 ± 4.5	6.6 ± 0.5	6.1 ± 3.5
$E_{\text{couplings}}$	1.3 ± 2.1	1.0 ± 0.3	1.5 ± 0.9
$E_{\text{dihedral angles}}$	0.33 ± 0.34	0.06 ± 0.08	0.32 ± 0.77
$E_{\text{improper angles}}$	9.7 ± 9.7	15.7 ± 4.3	9.5 ± 6.4
E_{NOE}	21 ± 20	29 ± 3	33 ± 19
E_{vdw}	7.9 ± 7.1	7.9 ± 1.1	15.7 ± 8.9
coordinate precision ^b (Å)			
rms deviation for selected heavy atoms ^c	0.23 , 0.15	0.26 , 0.18	0.66 , 0.30

^a Statistics are computed on sets of accepted structures from the 30 generated structures for each selected isomer subfamily (see Table 2). ^b The rms deviation calculated on sets of accepted structures. ^c Values in boldface type are computed with heavy atoms of the peptidic backbone, the chromophore with the exception of the succinate group, both hydroxyornithine side chains, and the Ga³⁺ ion. The values in lightface type are computed without the heavy atoms of the macrocycle.

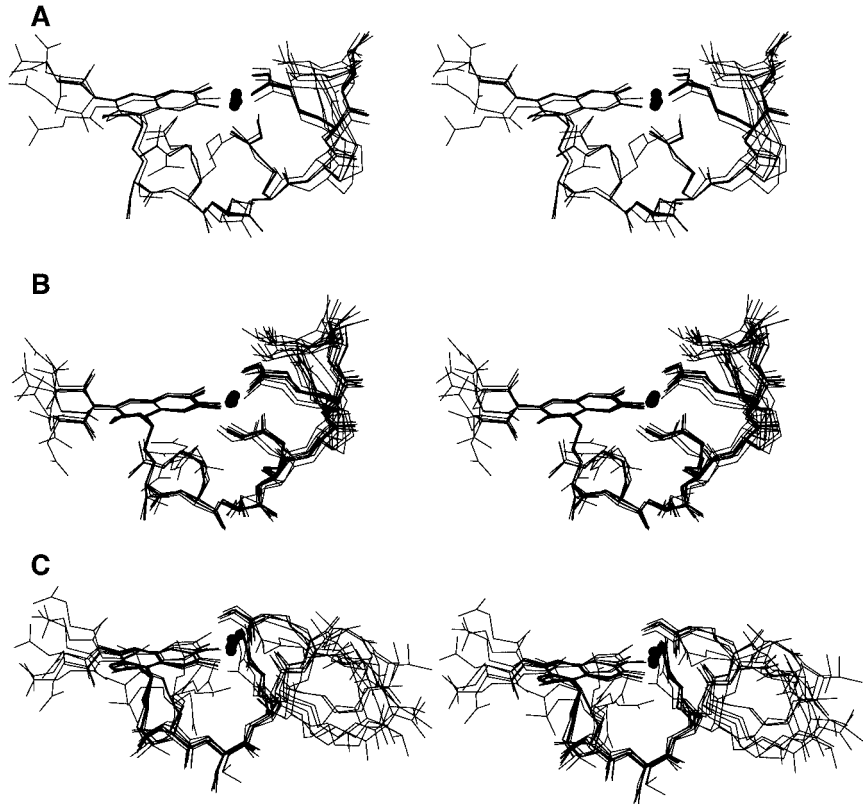


FIGURE 4: Wire representation and all-atom superimposition of low-NOE energy structures of PvdI. Convergent sets of structures were obtained for the A- Δ 7 (A), A- Δ 8 (B), and B- Λ 4 (C) conformers. The Ga³⁺ ion is represented by a dark sphere.

allowed the set of structures with an absolute Λ configuration to be discarded for the A conformer and those with the Δ configuration to be discarded for the B conformer. Two configurations (Δ 7 and Δ 8) remain for conformer A, while a single absolute configuration of the metal coordination center (Λ 4) was found to be compatible with the experimental restraints for conformer B. For conformer A, the two sets of convergent structures had rms deviation values (measured for heavy atoms) of 0.23 and 0.26 Å for the Δ 7 and Δ 8 configurations, respectively (Table 4 and Figure 4),

and the backbone atoms of these two configurations could be superimposed with a rms deviation value of 0.56 Å, reflecting the fact that the two configurations differ only in a permutation of the two metal-binding oxygen atoms of the L-FoOHOrn4 side chain, a subtle conformational change that could not be distinguished with the available data. In the following discussion, the Δ 8 configuration was selected since it gave slightly lower overall energies and better convergence. As expected from the smaller number of structural restraints (Table 1), conformer B is defined with less precision than

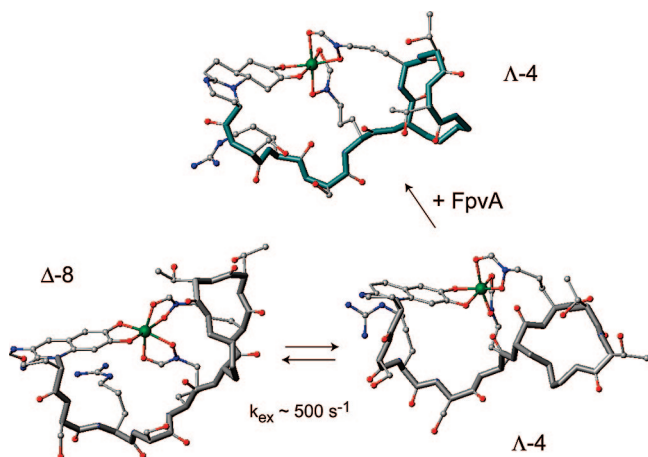


FIGURE 5: Comparison of A- Δ 8, B- Δ 4, and FpvAI-bond conformers of PvdI (11). The rate of exchange between the A- Δ 8 and B- Δ 4 conformers at room temperature is indicated.

conformer A, with a rms deviation of 0.66 Å. In particular, analysis of the set of structures shows lower precision in the cyclic C-terminal part of the peptide (Figure 4).

Comparison of Conformers A and B. A comparison between the two principal subfamilies of structures (A- Δ 8 and B- Δ 4) is shown in Figure 5. The global form of A- Δ 8 is characterized by a U-shaped cradle around the site of coordination with the peptidic backbone being held distant from the metal coordination sphere. After a sharp change of direction at L-Arg2, the peptide chain rolls smoothly around the metal. The guanidinium group of L-Arg2 has a well-defined position and stacks under the chromophore ring. In this conformation, the C-terminal residues (L-Thr7 and L-Thr8) lie well above the plane defined by the chromophore and the gallium ion. The side chains of the two gallium-binding hydroxyornithine residues (L-FoOHOrn4 and L-FoOHOrn6) are in an extended conformation, which maintains the peptide backbone far from the coordination sphere. It is worth noting that the polar residues (i.e., D-Ser1, D-Ser3, L-Thr7, and L-Thr8) are all oriented toward the solvent, contributing to complex solubilization.

For the B- Δ 4 conformer, the macrocycle formed by the covalent bond between L-Thr8 and L-Lys5 is oriented away from the metal coordination site. This leads to a more extended structure: the main axis of the molecule is 13.6 Å in length for the B- Δ 4 conformer, compared to 12.0 Å in the A- Δ 8 conformer. The L-Arg2 side chain is again located below the plane of the chromophore, but in a position that is more exposed to solvent than in the A- Δ 8 conformer. Polar side chains are again oriented toward the solvent. The main consequence of the orientation of the macrocycle observed in the B- Δ 4 conformer is a more open environment for the metal ion. In this configuration, the siderophore masks less than one-eighth of the surface of the sphere of the gallium(III) ion.

Diffusional Properties of the Two Conformations. The two conformers of PvdI-Ga(III) have quite different overall shapes which is expected to be reflected in their diffusional properties. To probe differences in the rotational diffusion tensors of the two conformers, ^{15}N relaxation parameters were measured at 253 K. The longitudinal (R_1) and transverse (R_2) relaxation rates and the heteronuclear ^1H – ^{15}N NOE measured for the two conformers are shown in Figure 6. The profile of R_1 values along the peptide chain shows consis-

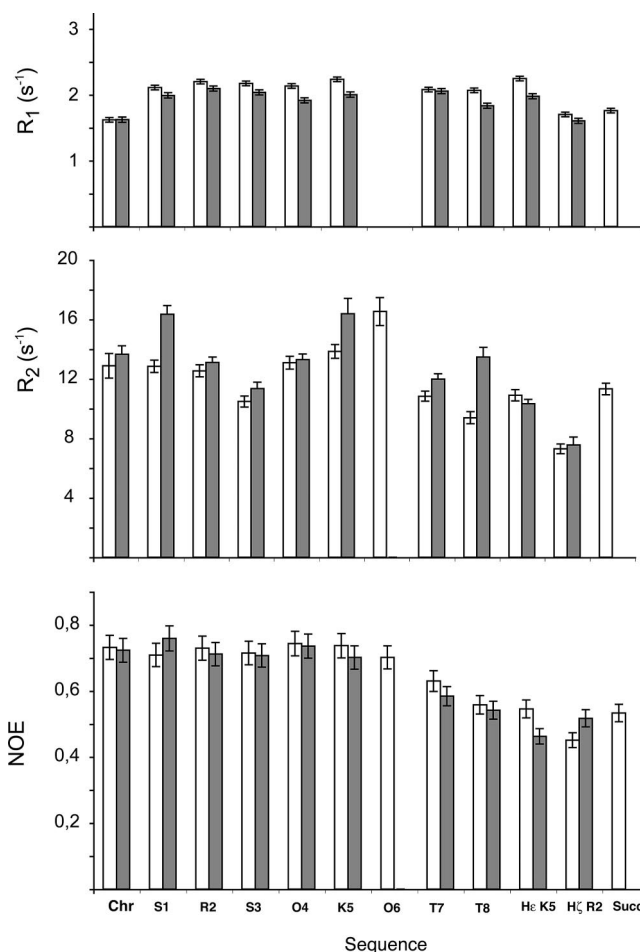


FIGURE 6: Longitudinal and transverse relaxation rates together with ^1H – ^{15}N heteronuclear NOE values measured for the two conformers of PvdI-Ga(III) (data for conformer A in light gray and data for conformer B in dark gray). Only one set of resonances was observed for the succinate group (Succ), leading to a single set of relaxation data. For residue L-FoOHOrn6, relaxation rates could be measured for only the A conformer.

tently lower values for the B- Δ 4 conformer. The opposite is observed for R_2 values, with most residues of the B- Δ 4 conformer displaying higher relaxation rates than the same residues in the A- Δ 8 conformer. It should be noted that the high transverse relaxation rates observed for amide ^{15}N nuclei of L-Arg2, L-Lys5, and L-Thr8 in the B- Δ 4 conformer may be the result of micro- to millisecond time scale exchange contributions. Nevertheless, the clear and consistent trends in the relaxation rates indicate a longer correlation time for overall tumbling for the B- Δ 4 conformer. Analysis of the heteronuclear NOE profiles on the other hand reveals similar values for the two conformers, suggesting conserved fast pico- to nanosecond time scale motions. The flat profile for residues from D-Ser1 to L-Lys5 with values of the heteronuclear NOE of 0.72 indicates restricted internal motions on this time scale for this portion of the peptidic chain. In contrast, for the backbone ^{15}N nuclei of residues of the macrocycle, L-Thr7 and L-Thr8, and the side chain $^{15}\text{N}\zeta$ nucleus of L-Lys5, lower values of the NOE indicate larger amplitudes of pico- to nanosecond time scale internal motions. Consistently lower values of the heteronuclear NOE for these residues measured for the B- Δ 4 conformer might indicate enhanced fast dynamics for the macrocycle of this conformer. The side chain $^{15}\text{N}\epsilon$ nucleus of L-Arg2 has

similarly low values for the NOE, although lower values would be expected for a side chain with unrestricted motions.

Since the linear part of the peptide shows limited internal motions, data for these residues were used to estimate the correlation times for the two conformers using the ratio between transverse and longitudinal relaxation rates, R_2/R_1 . Values of 8.5 ± 1.0 and 9.3 ± 1.0 ns were obtained for conformers A- $\Delta 8$ and B- $\Delta 4$, respectively. These high values of the correlation times are due to the viscosity of the cryosolvent and are in agreement with the values calculated from homonuclear NOE buildup curves for the pair of chromophore protons, H4 and H5. Indeed, the cross-relaxation rates measured for this fixed distance vector were -2.27 ± 0.06 and $-2.62 \pm 0.28 \text{ s}^{-1}$, leading to correlation times of 8.0 ± 0.3 and 9.3 ± 1.0 ns for the A- $\Delta 8$ and B- $\Delta 4$ conformers, respectively. The larger values obtained for the B- $\Delta 4$ conformer are consistent with its larger dimensions that result from the open position of the macrocycle.

DISCUSSION

The complex formed by pyoverdine PvdI from *P. aeruginosa* with metal ions exhibits exchange between two conformers with roughly equivalent populations, in solution. The rate associated with this exchange process is such that resonances in the ^1H NMR spectrum of PvdI-Ga(III) are severely broadened at ambient temperature, and although two sets of resonances can be distinguished at lower temperatures, exchange contributions to NOEs prohibit structure determination in aqueous solution. By using cryosolvents, the sample temperature could be lowered to 253 K, where NMR observables (chemical shifts, relaxation rates) are in the slow exchange regime, and triple-resonance experiments normally applied to proteins yielded full resonance assignments (20). At 253 K, exchange contributions to NOEs are reduced sufficiently for peak intensities to be interpreted in terms of internuclear distances and for the structure of each of the exchanging conformers to be determined.

Structure calculations were performed for each conformer, using a strategy that was successfully applied previously in defining both the structure of the peptide chain and the absolute configuration of the metal coordination sphere of two other peptidic siderophores: pyoverdine G4R from *P. putida* (8) and azoverdin from *A. macrocytogenes* ATCC 12334 (9). In the case of PvdI-Ga(III), this procedure yielded two configurations compatible with experimental data for conformer A (A- $\Delta 7$ and A- $\Delta 8$) and a single configuration (B- $\Delta 4$) for conformer B. The two solutions for conformer A are very similar, differing only in a rotation about the C δ –N ϵ bond of L-FoOHOrn4, thus altering the orientation of the coordinating functional group with respect to the metal ion but having little effect on the peptide backbone. Most probably, only one of these configurations is present in solution, but the structural data (distances and angles) close to the metal ion are relatively poor and do not allow us to discriminate between these two forms. In previous studies of pyoverdines, a single solution for the absolute configuration of the coordination sphere was obtained (8, 9). In the case of azoverdin, however, the metal chelating groups are located at the end of long hydroxyornithine side chains, as in PvdI, leading to an ambiguity that could only be resolved using residual dipolar couplings (9). No suitable alignment

medium could be found for the measurement of residual dipolar couplings for PvdI-Ga(III) at 253 K that would have allowed further refinement of the structures.

The configurations of the metal coordination sphere in conformers A and B of PvdI-Ga(III) have opposite chiralities (Δ and Λ , respectively). Exchange between these two configurations is associated with a major structural rearrangement of the macrocycle, resulting in differences in chemical shifts for nearly all ^1H , ^{15}N , and ^{13}C nuclei of the molecule and a subtle but detectable difference in the rotational diffusion properties. The measurement of exchange kinetics at several temperatures allowed us to evaluate the activation enthalpy for exchange as 20 kcal/mol, a value that is compatible with the break of one oxygen–metal bond. The observation that exchange rates depend on the nature of the metal supports the argument for an exchange process that involves a change in metal coordination. Indeed, the larger crystal field stabilization energy of the octahedral d^3 chromic ion slows the coordination sphere isomerization to such an extent that the conformers of PvdI-Cr(III) could be separated chromatographically (18). The two products gave different circular dichroism (CD) spectra, suggesting different absolute configurations. Racemization of gallium complexes has been reported for a catechol siderophore analogue (26) and for the citrate-based siderophores acinetoferrin and schizokinen (28), with activation enthalpies of 14 and 25 kcal/mol, respectively, bracketing the value measured in this study (20 kcal/mol). For metal complexes of PvdI, the stepwise mechanism of this isomerization remains to be elucidated. However, the detection of micro- to millisecond time scale exchange that broadens the amide proton resonance of L-FoOHOrn6 in conformer B suggests that breakage of one of the L-FoOHOrn6–Ga $^{3+}$ bonds might be involved in this racemization process.

This work has produced the first three-dimensional structure of a pyoverdine with a partially cyclic peptide moiety, and the two resulting structures, which add to a rather small set of peptidic siderophore structures, further emphasize the structural diversity of this class of siderophores. Each siderophore meets the requirement for binding metal ions with exceptionally high affinity such that the resulting complex is recognized by a specific receptor at the level of the outer membrane. Common features can begin to be identified from a comparison of these structures.

(i) The hydroxylated residues, such as serine and threonine residues, which are common in pyoverdines are consistently oriented toward the solvent, playing an important role in the solvation of the complex.

(ii) The peptide chains wrap around the metal ion but leave a large accessible space to the metal ion. The orientation of this open path to the metal differs among the pyoverdine structures, suggesting that the positioning of the peptide chain relative to the metal constitutes one of the structural features that confers specific recognition by the receptor.

Despite the availability of a number of outer membrane receptors, no general features of the interactions have yet been defined (28). The binding site is formed by residues located both in extracellular loops of the β barrel and within the plug domain which obstructs the passage through the barrel. Comparison of receptor–siderophore complexes of citrate (29) and ferrichrome (30) indicated a different nature of the specific amino acids involved in the binding. Elec-

trostatic interactions appear to play an important role in citrate recognition with the binding pocket of FecA being lined with positively charged residues, whereas the corresponding regions of FhuA and FepA are predominantly lined with aromatic and/or hydrophilic residues. For metal-bound PvdI, the strikingly well-defined position of L-Arg2, stacked below the chromophore ring, correlates with its involvement in receptor binding through an electrostatic interaction with Asp597 of FpvAI (15). When PvdI binds to FpvAI, the hydroxyl groups of the residues of PvdI remain mostly exposed to solvent whereas the large accessible space to the ion observed in our structures becomes filled by aromatic residues of FpvAI located in one loop of the β barrel, namely, Phe795 and Tyr796.

Further insight into the structural determinants of pyoverdine–receptor recognition can be gained from a comparison of the structure of pyoverdine PvdI–Fe(III) bound to the FpvAI receptor (Figure 5) (15) and the solution structure of PvdI–Ga(III). In the crystal structure of the FpvAI–PvdI–Fe(III) complex, only the Λ -4 configuration was observed for the receptor-bound pyoverdine, suggesting that one of the two conformers that interconvert in solution is selected by the receptor. The stereospecificity of iron uptake systems has been observed previously for other siderophore receptors such as the pyochelin receptor (31) and suggests a possible mechanism for preventing competitors from hijacking the iron uptake system.

Further comparison of PvdI–Ga(III) in solution and PvdI–Fe(III) bound to the FpvAI receptor reveals a distinct change in the peptide backbone conformation upon binding to the receptor, most notably involving residues L-Lys5–L-Thr8 of the macrocycle. This flexibility of the macrocycle, which was detected by heteronuclear relaxation experiments, may serve to define a specific feature of metal-bound PvdI that is recognized by the FpvAI receptor. This dynamical behavior, which has also been observed in regions neighboring the binding pocket of the receptor, suggests an induced fit mechanism that may trigger further conformational transitions to allow the pyoverdine to be translocated into the periplasm.

CONCLUSION

We have shown that pyoverdine PvdI from *P. aeruginosa* adopts two exchanging conformations upon binding the diamagnetic gallium(III) ion. At 253 K, the rate of conformational exchange is sufficiently slow to allow conformation-specific NMR restraints to be measured and three-dimensional structures to be calculated. The set of resulting structures indicates that the observed conformational exchange involves a stereoisomerization of the metal binding coordination accompanied by a change in the global shape of the siderophore. This change, which affects the rotational diffusion properties of the pyoverdine, was further characterized by heteronuclear ^{15}N relaxation measurements. One of the conformers found in solution is present in the crystal structure of the complex of PvdI with its specific outer membrane receptor FpvAI, an observation which suggests a possible stereoselection mechanism during the siderophore–receptor interaction.

ACKNOWLEDGMENT

Isabelle Schalk and Gaëtan Mislin are acknowledged for helpful discussions. We thank Claude Ling for maintenance of NMR spectrometers and IGBMC common facilities.

SUPPORTING INFORMATION AVAILABLE

Initial distances and cross-relaxation rates σ . This material is available free of charge via the Internet at <http://pubs.acs.org>.

REFERENCES

- Andrews, S. C., Robinson, A. K., and Rodriguez-Quinones, F. (2003) Bacterial iron homeostasis. *FEMS Microbiol. Rev.* 27, 215–237.
- Boukhalfa, H., and Crumbliss, A. L. (2002) Chemical aspects of siderophore-mediated iron transport. *BioMetals* 15, 325–339.
- Neilands, J. B. (1982) Microbial envelope proteins related to iron. *Annu. Rev. Microbiol.* 36, 285–309.
- Pattus, F., and Abdallah, M. A. (2000) Siderophores and Irons: Transport in Microorganisms. *J. Chin. Chem. Soc.* 47, 1–20.
- Meyer, J. M. (2000) Pyoverdines: Pigments, siderophores and potential taxonomic markers of fluorescent *Pseudomonas* species. *Arch. Microbiol.* 174, 135–142.
- Teintze, M., Hossain, M. B., Barnes, C. L., Leong, J., and van der Helm, D. (1981) Structure of ferric pseudobactin, a siderophore from a plant growth promoting *Pseudomonas*. *Biochemistry* 20, 6446–6457.
- Mohn, G., Koehl, P., Budzikiewicz, H., and Lefèvre, J. F. (1994) Solution Structure of Pyoverdin Gm-II. *Biochemistry* 33, 2843–2851.
- Atkinson, R. A., El Din, A., Kieffer, B., Lefèvre, J. F., and Abdallah, M. A. (1998) Bacterial iron transport: H-1 NMR determination of the three-dimensional structure of the gallium complex of pyoverdin G4R, the peptidic siderophore of *Pseudomonas putida* G4R. *Biochemistry* 37, 15965–15973.
- Wasielowski, E., Atkinson, R. A., Abdallah, M. A., and Kieffer, B. (2002) The three-dimensional structure of the gallium complex of azoverdin, a siderophore of *Azomonas macrocytogenes* ATCC 12334, determined by NMR using residual dipolar coupling constants. *Biochemistry* 41, 12488–12497.
- Demange, P., Wendenbaum, S., Linget, C., Mertz, C., Cung, M. T., Dell, A., and Abdallah, M. A. (1990) Bacterial siderophores: Structure and NMR assignment of pyoverdins Pa, siderophores of *Pseudomonas aeruginosa* ATCC 15692. *BioMetals* 3, 155–170.
- Schalk, I. J., Kyslik, P., Prome, D., van Dorselaer, A., Poole, K., Abdallah, M. A., and Pattus, F. (1999) Copurification of the FpvA ferric pyoverdin receptor of *Pseudomonas aeruginosa* with its iron-free ligand: Implications for siderophore-mediated iron transport. *Biochemistry* 38, 9357–9365.
- Schalk, I. J., Dugave, C., Poole, K., Abdallah, M. A., and Pattus, F. (2001) Iron-free pyoverdin binds to its outer membrane receptor FpvA in *Pseudomonas aeruginosa*: A new mechanism for membrane iron transport. *Mol. Microbiol.* 39, 351–361.
- Schons, V., Atkinson, R. A., Dugave, C., Graff, R., Mislin, G. L., Rochet, L., Hennard, C., Kieffer, B., Abdallah, M. A., and Schalk, I. J. (2005) The structure-activity relationship of ferric pyoverdine bound to its outer membrane transporter: Implications for the mechanism of iron uptake. *Biochemistry* 44, 14069–14079.
- Cobessi, D., Celia, H., Folschweiller, N., Schalk, I. J., Abdallah, M. A., and Pattus, F. (2005) The crystal structure of the pyoverdine outer membrane receptor FpvA from *Pseudomonas aeruginosa* at 3.6 angstroms resolution. *J. Mol. Biol.* 347, 121–134.
- Wirth, C., Meyer-Klaucke, W., Pattus, F., and Cobessi, D. (2007) From the periplasmic signaling domain to the extracellular face of an outer membrane signal transducer of *Pseudomonas aeruginosa*: Crystal structure of the ferric pyoverdine outer membrane receptor. *J. Mol. Biol.* 368, 398–406.
- Clément, E., Mesini, P. J., Pattus, F., and Schalk, I. J. (2004) The binding mechanism of pyoverdin with the outer membrane receptor FpvA in *Pseudomonas aeruginosa* is dependent on its iron-loaded status. *Biochemistry* 43, 7954–7965.
- Mertz, C., Demange, P., Marraud, M., Dell, A., Linget, C., Abdallah, M. A., and Cung, M. T. (1991) Conformational study

- of the Al(III)-Pyoverdin complex from *Pseudomonas aeruginosa* by ^1H 2D NMR techniques. *Peptides*, 543–544.
18. Budzikiewicz, H., Georgias, H., and Taraz, K. (2002) Diastereomeric pyoverdin-chromium(III) complexes. *Z. Naturforsch. C57*, 954–956.
 19. Folschweiller, N., Gallay, J., Vincent, M., Abdallah, M. A., Pattus, F., and Schalk, I. J. (2002) The interaction between pyoverdin and its outer membrane receptor in *Pseudomonas aeruginosa* leads to different conformers: A time-resolved fluorescence study. *Biochemistry* 41, 14591–14601.
 20. Tzou, D. L., Wasielewski, E., Abdallah, M. A., Kieffer, B., and Atkinson, R. A. (2005) A low-temperature heteronuclear NMR study of two exchanging conformations of metal-bound pyoverdin PaA from *Pseudomonas aeruginosa*. *Biopolymers* 79, 139–149.
 21. Kuboniwa, H., Grzesiek, S., Delaglio, F., and Bax, A. (1994) Measurement of HN-H α J couplings in calcium-free calmodulin using new 2D and 3D water-flip-back methods. *J. Biomol. NMR* 4, 871–878.
 22. Farrow, N. A., Muhandiram, R., Singer, A. U., Pascal, S. M., Kay, C. M., Gish, G., Shoelson, S. E., Pawson, T., Forman-Kay, J. D., and Kay, L. E. (1994) Backbone dynamics of a free and phosphopeptide-complexed Src homology 2 domain studied by ^{15}N NMR relaxation. *Biochemistry* 33, 5984–6003.
 23. Schwieters, C. D., Kuszewski, J. J., Tjandra, N., and Clore, G. M. (2003) The Xplor-NIH NMR molecular structure determination package. *J. Magn. Reson.* 160, 65–73.
 24. Nilges, M., Clore, G. M., and Gronenborn, A. M. (1988) Determination of three-dimensional structures of proteins from inter-proton distance data by dynamical simulated annealing from a random array of atoms. *FEBS Lett.* 239, 129–136.
 25. Koradi, R., Billeter, M., and Wuthrich, K. (1996) MOLMOL: A program for display and analysis of macromolecular structures. *J. Mol. Graphics* 14, 51–55.
 26. Kersting, B., Telford, J. R., Meyer, M., and Raymond, K. N. (1996) Gallium(III) catecholate complexes as probes for the kinetics and mechanism of inversion and isomerization of siderophore complexes. *J. Am. Chem. Soc.* 118, 5712–5721.
 27. Fadeev, E. A., Luo, M. K., and Groves, J. T. (2004) Synthesis, structure, and molecular dynamics of gallium complexes of schizokinen and the amphiphilic siderophore acinetoferrin. *J. Am. Chem. Soc.* 126, 12065–12075.
 28. Chakraborty, R., Storey, E., and van der Helm, D. (2007) Molecular mechanism of ferricsiderophore passage through the outer membrane receptor proteins of *Escherichia coli*. *BioMetals* 20, 263–274.
 29. Ferguson, A. D., Chakraborty, R., Smith, B. S., Esser, L., van der Helm, D., and Deisenhofer, J. (2002) Structural basis of gating by the outer membrane transporter FecA. *Science* 295, 1715–1719.
 30. Locher, K. P., Rees, B., Koebnik, R., Mitschler, A., Moulinier, L., Rosenbusch, J. P., and Moras, D. (1998) Transmembrane signaling across the ligand-gated FhuA receptor: Crystal structures of free and ferrichrome-bound states reveal allosteric changes. *Cell* 95, 771–778.
 31. Youard, Z. A., Mislin, G. L. A., Majcherczyk, P. A., Schalk, I. J., and Reimann, C. (2007) *Pseudomonas fluorescens* CHA0 produces enantio-pyochelin, the optical antipode of the *Pseudomonas aeruginosa* siderophore pyochelin. *J. Biol. Chem.* 282, 35546–35553.

BI702214S